International Journal of Heat and Mass Transfer 52 (2009) 5055–5063

Contents lists available at ScienceDirect

International Journal of Heat and Mass Transfer

journal homepage: www.elsevier.com/locate/ijhmt

Mixed convective heat transfer in rectangular enclosures driven by a continuously moving horizontal plate

M.A. Waheed

Mechanical Engineering Department, Ladoke Akintola University of Technology, P.M.B. 4000 Ogbomoso, Oyo State, Nigeria

ARTICLE INFO

Article history:
Received 6 June 2008
Accepted 21 May 2009
Available online 21 June 2009

Keywords:
Mixed convection
Heat transfer
Buoyancy effect
Stream function
Isotherms
Finite difference scheme

ABSTRACT

The fluid flow and heat transfer induced by the combined effects of the mechanically driven lid and the buoyancy force within rectangular enclosures were investigated in this work. The fluid filled enclosures are heated and lid-driven either on the upper or on the lower horizontal wall, thermally isolated on the right vertical wall, and cooled on the other walls. The basis of the investigation was the numerical solutions of the equations for the conservation of mass, momentum, and energy transport using the finite difference method. The effects of the flow governing parameters including the Richardson and the Prandtl numbers, and the length-to-height aspect ratio, respectively, in the range $10^{-2} \leqslant Ri \leqslant 10^{2}$, $10^{-3} \leqslant Pr \leqslant 10$, and $1 \leqslant AR \leqslant 4$ for a fixed Reynolds number, $Re = 100$, were studied. The results are presented in the form of the hydrodynamic and thermal fields, and the profiles for vertical and horizontal components of velocity, temperature, and the local heat flux. The fluid flow and energy distributions within the enclosures and heat flux on the heated wall are enhanced by the increase in the Richardson number. While an increase in the Prandtl number improves the heat flux on the heated wall, an increase in aspect ratio suppresses it. The results can be used as base line data in the design of systems in which mixed convection heat transfer in rectangular enclosures occurs.

1. Introduction

The problem of heat transfer by mixed convection has been the subject of intensive theoretical, numerical, and experimental investigations in the recent years because of its significant applications in nature and in many scientific and engineering practices. The analysis of mixed convective flow in a lid-driven cavity finds applications in flow and heat transfer in solar ponds and solar collectors, dynamics of lakes, reservoirs and cooling ponds, cooling of electronic systems, thermal-hydraulics of nuclear reactors, thermal convection in micropolar fluids, chemical processing equipment, lubricating grooves, crystal growing, materials processing such as float glass production, galvanizing, metal coating and casting, food processing, and industrial processes where a solid ribbon or a solid material is heated as it moves through a furnace, among others [1–7]. Results of extensive two- and three-dimensional numerical computational studies of the lid-driven flow are available in the literature [1,3–13], and the consistency between these numerical predictions and laboratory experiments [14–16] has been explained.

The analysis of heat transfer by mixed convection in lid-driven cavity is very complex due to the interaction of the shear driven force and the buoyancy effects. The flow governing dimensionless parameter is the Richardson number, Ri, defined as the ratio of the Grashof number, Gr, to the square of the Reynolds number, Re, i.e. $Ri = Gr/Re^2$. The Richardson number is a measure of the relative importance of the buoyancy-driven natural convection to the lid-driven forced convection. Depending on the values of the Richardson number, the problem of the combined shear and buoyancy-driven convection can be classified into three flow regimes as follows; pure forced convection for $Ri \ll 1$, mixed convection for $0.1 \leqslant Ri \leqslant 10$, and pure natural convection for $Ri \gg 1$ [1,4,17]. The characterization of the two limiting flow regimes viz., forced and natural convection is very essential for the complete understanding of the mechanism of the mixed convection problem from the technical and engineering standpoints. The two competing convection mechanisms are also determined by the choice of Reynolds number and Prandtl number [4].

Many investigators have studied mixed convective heat transfer in different configurations and combinations of thermal boundary conditions that idealized problems encountered in many practical engineering and industrial applications. Such configurations can be idealized by the simple rectangular geometry with regular boundary conditions yielding a well-posed problem. A search of the literature reveals that the studies of lid-driven cavity can broadly be classified into two configurations. The effects of dimensionless parameters including the Reynolds number, Grashof number, Prandtl number, the cavity orientation and the aspect ratio have been studied numerically for the flow induced by both shear and buoyancy in the rectangular cavities.

E-mail addresses: adekojo.waheed@daad-alumni.de, akindoye@yahoo.com

0017-9310/$ - see front matter © 2009 Published by Elsevier Ltd.
doi:10.1016/j.ijheatmasstransfer.2009.05.011

Nomenclature

AR	length-to-height aspect ratio (= L/H)
c_p	specific heat capacity of fluid
g	acceleration due to gravity
Gr	Grashof number (= $g\beta(T_w - T_c)L^3/\nu^2$)
H	height of the enclosure
h	heat transfer coefficient
k	fluid thermal conductivity
L	length of the enclosure
M	number of horizontal grid lines
n	number of iterations
N	number of vertical grid lines
Nu	average Nusselt number ($= \dot{Q}/k\Delta T = hL/k$)
Nu_x	local Nusselt number
p	pressure
Pr	Prandtl number (= ν/ρ)
$\dot{Q}$	overall heat transfer rate
Ra	Rayleigh number (= $GrPr = g\beta(T_w - T_c)L^3/\alpha\nu$)
Re	Reynolds number (= U_wL/ν)
Ri	Richardson number (= $Gr/Re^2 = \beta(T_w - T_c)L/U_w^2$)
t	time
T	temperature
u	horizontal velocity component
U	dimensionless horizontal velocity component
v	vertical velocity component
V	dimensionless vertical velocity component
x	horizontal coordinate
X	dimensionless horizontal coordinate
y	vertical coordinate
Y	dimensionless vertical coordinate

Greek alphabet

α	fluid thermal diffusivity ($\alpha = k/\rho c_p$)
β	volumetric coefficient of thermal expansion
δ	residual value
μ	viscosity
ν	kinematic viscosity
θ	dimensionless temperature ($(T - T_c)/(T_w - T_c)$)
ρ	density
τ	dimensionless time
ω	vorticity
Ω	dimensionless vorticity
ψ	stream function
Ψ	dimensionless stream function

Sub- and superscripts

w	condition of moving wall
c	condition of ambient medium

The most widely studied configuration appearing in the literature is the one in which the forced convection is induced by the uniform motion of a single, or two opposite side walls while the horizontal walls are thermally insulated [1,4,9–11]. Aydin [1] investigated the effect of aiding- and opposing buoyancy on the mixed convection for the case of one single moving vertical wall. He discovered that the range of Richardson number for opposing buoyancy case was wider than that of the aiding-buoyancy case, although he did not present any quantitative information regarding these regimes and heat transfer characteristics. The two vertical walls in the configuration investigated by Oztop and Dagtekin [7] were set into motion. The results revealed that for $Ri < 1$ the influence of moving walls on the heat transfer is the same when they move in opposite direction regardless of which side moves upwards and is reduced when both move upwards. For the case of opposing buoyancy and shear forces and for $Ri > 1$, the heat transfer is somewhat better due to formation of secondary cells on the walls and a counter rotating cell at the center. Ghasemi and Aminossadati [11] investigated the unsteady laminar mixed convection heat transfer in a cavity subjected to heating on a fraction of the left vertical wall while the right vertical wall slides with either a constant or an oscillating velocity. The results indicate that the direction and magnitude of the velocity of the sliding wall affect the heat transfer rate.

Aydin and Yang [9] investigated the heat transfer mechanism on a laminar mixed convection in a shear- and buoyancy-driven cavity with the fraction of its lower wall heated and cooled from moving upper wall. They found out that for the ratio of the length of the heated portion of the lower wall to the entire length of the enclosure, equals to 0.2, the mixed convection region with comparable shear and buoyancy forces is more effective for the range $0.5 \leqslant Ri \leqslant 2$, which increases with the ratio. Depending on their relative directions to the direction of inertia-driven flow, the buoyancy forces may aid or oppose the forced flow, causing an increase or decrease in heat transfer rates.

The other well studied configuration in lid-driven cavity is the case of a single, or two opposite horizontal walls, sliding at a constant velocity or oscillatory, while the side walls are thermally insulated [3,8,12,13,18–21]. From the parametric investigation carried out by Iwatsu et al. [18] in a square cavity and, Mohamad and Viskanta [8] in a three-dimensional shallow cavity with the upper wall at higher temperature than the lower stationary wall, they discovered that the recirculation flow is confined to the upper region while the heat transfer in the lower region is dominated by conduction. Luo and Yang [12] investigated the effect of Grashof and Reynolds numbers on flow stability in a flow in which the top and bottom lids of the cavity move in opposite directions and are at different temperature for an aspect ratio of 1.96. Sharif [3] investigated the effects of the inclination of the cavity on the flow and thermal fields in addition to the effects of Rayleigh and Richardson numbers for an aspect ratio of 10. The average Nusselt number is found to increase mildly with the cavity inclination for dominating forced convection case and steeply in dominating natural convection case. Khanafer et al. [13] investigated the effects of oscillatory motion of the upper wall. Their obtained results reveal that the Reynolds and Grashof numbers would either enhance or retard the energy transport process and drag force behaviour depending on the conduct of the velocity cycle. Small lid oscillation values are found to constrain the lid associated motion to a shallow depth from the sliding lid plane.

A review of the available literature shows that the convective heat transfer and flow in a rectangular enclosure driven by a horizontal wall while being cooled from one horizontal and vertical wall, with the other vertical wall thermally isolated have not been investigated. This configuration finds practical applications in the cooling of an extruded plate in a hot rolling process. The fluid flow and the heat transfer patterns within the enclosure dictate the degree of cooling and hence the quality of the final product. This fact motivates the present study. The purpose of this work is therefore to present a parametric investigation of the Richardson and Prandtl numbers, and the aspect ratio on the flow patterns, energy distribution and heat transfer behaviour for this configuration.

2. Problem analysis

The physical system being considered consists of a continuously moving horizontal plate emerging from a slot at a uniform velocity U_w and at temperature T_w into an otherwise quiescent fluid contained in an enclosure. The horizontal plate divides the rectangular enclosure into two equal halves. The problem domain is thus idealized to consist of two separate rectangular enclosures with the plate serving as the upper and lower bound of each equal halve (see Fig. 1). The enclosures are also bounded by a fixed horizontal wall on the lower and upper parts of the control domain, a fixed vertical wall bordering the extrusion die surface on the left and an adiabatic vertical wall on the right. The temperature, T_c, of the upper and lower horizontal walls, and that of the vertical wall bordering the extrusion die surface (i.e. the left vertical wall), is lower than that of the plate (i.e. $T_c < T_w$). The enclosures are filled with a quenching medium, the choice of which depends upon the material being quenched and the rate of cooling which is above the critical cooling rate to avoid cracking and distortion of the finished product. The quenching medium transports heat from the extruded material to the surrounding. The no-slip boundary conditions are adopted for velocities, thus the horizontal and vertical velocity components, are set to zero at the stationary walls, and to the specified velocity at the moving plate.

The flow of the enclosed fluid is considered to be two-dimensional, steady, incompressible, and laminar. The fluid is assumed to be Newtonian with all the fluid properties taken as constant except for the density variation with temperature for which the Boussinesq approximation is used. The heat transfer by radiation and the internal heat generation are assumed negligible. The governing equations for the system of the enclosed fluid are the expression for the conservation of mass, momentum, and energy transports at every point of the system within the limit of the basic assumptions and the use of appropriate boundary conditions.

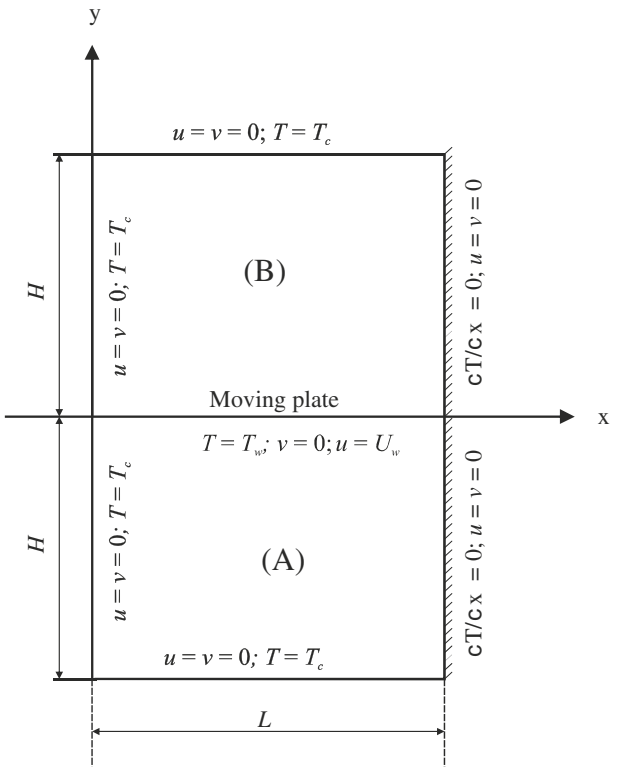

Fig. 1. Schematic representation of the physical model with the boundary constraints and the coordinate axes.

These equations which can be seen in any classical textbook of fluid dynamics such as the one from Schlichting and Gersten [22] are stated for a two-dimensional rectangular domain in Cartesian coordinates as follows:

The continuity equation:

$$\frac{\partial u}{\partial x} + \frac{\partial v}{\partial y} = 0. \tag{1}$$

The momentum equations, respectively, in the x- and y-directions:

$$\frac{\partial u}{\partial t} + u\frac{\partial u}{\partial x} + v\frac{\partial u}{\partial y} = -\frac{1}{\rho}\frac{\partial p}{\partial x} + \nu\left(\frac{\partial^2 u}{\partial x^2} + \frac{\partial^2 u}{\partial y^2}\right), \tag{2}$$

$$\frac{\partial v}{\partial t} + u\frac{\partial v}{\partial x} + v\frac{\partial v}{\partial y} = -\frac{1}{\rho}\frac{\partial p}{\partial y} + \nu\left(\frac{\partial^2 v}{\partial x^2} + \frac{\partial^2 v}{\partial y^2}\right) + \beta g(T - T_c), \tag{3}$$

where $\beta g(T - T_c)$ stands for the buoyancy force term which is the body force per unit volume in the y-direction. The Boussinesq approximation for density variation with temperature is expressed as

$$\rho = \rho_c(1 - \beta(T - T_c)). \tag{4}$$

The thermal energy transport equation is:

$$\rho c_p\left(\frac{\partial T}{\partial t} + u\frac{\partial T}{\partial x} + v\frac{\partial T}{\partial y}\right) = k\left(\frac{\partial^2 T}{\partial x^2} + \frac{\partial^2 T}{\partial y^2}\right). \tag{5}$$

In the above equations, the parameter ρ denotes the fluid density, c_p the specific heat capacity at constant pressure, μ the fluid viscosity, k the thermal conductivity, t the time, T the temperature, u and v are the fluid velocity components, respectively, in x- and y-directions, p the pressure, and β the volumetric coefficient of thermal expansion.

The Navier–Stokes equations (2) and (3) are reduced into one elliptic and one parabolic non-dimensional equation by the introduction of the expressions describing the velocity components as the derivatives of the stream function,

$$u = \frac{\partial \psi}{\partial y}, \quad v = -\frac{\partial \psi}{\partial x}, \tag{6}$$

the vorticity equation,

$$\omega = \frac{\partial v}{\partial x} - \frac{\partial u}{\partial y}, \tag{7}$$

and the dimensionless parameters,

$$X = \frac{x}{L}, \quad Y = \frac{y}{L}, \quad U = \frac{u}{U_w}, \quad V = \frac{v}{U_w}, \quad \tau = \frac{tU_w}{L},$$
$$\theta = \frac{T - T_c}{T_w - T_c}, \quad \Psi = \frac{\psi}{U_w L}, \quad \Omega = \frac{\omega}{U_w/L}, \tag{8}$$

where ω and ψ stand for the dimensional vorticity and stream function, respectively, U_w is the plate velocity and L is the length of the enclosure.

The results of the analysis are the stream function equation describing the flow kinematics:

$$\Omega = -\left(\frac{\partial^2 \Psi}{\partial X^2} + \frac{\partial^2 \Psi}{\partial Y^2}\right) \tag{9}$$

and the vorticity transport equation [12,23]

$$\frac{\partial \Omega}{\partial \tau} + U\frac{\partial \Omega}{\partial X} + V\frac{\partial \Omega}{\partial Y} = \frac{1}{Re}\left(\frac{\partial^2 \Omega}{\partial X^2} + \frac{\partial^2 \Omega}{\partial Y^2}\right) + Ri\frac{\partial \theta}{\partial X}. \tag{10}$$

The energy equation (5) is also non-dimensionalized to give

$$\frac{\partial \theta}{\partial \tau} + U\frac{\partial \theta}{\partial X} + V\frac{\partial \theta}{\partial Y} = \frac{1}{RePr}\left(\frac{\partial^2 \theta}{\partial X^2} + \frac{\partial^2 \theta}{\partial Y^2}\right) \tag{11}$$

The principal non-dimensional parameters appearing in the above equations are the Reynolds number, *Re*, the Prandtl number, *Pr*, and the Richardson number, *Ri*.

In this work, the problem governing equations (9)–(11) are solved numerically with the prescribed boundary conditions for the velocity, stream function, vorticity, and temperature fields in dimensionless form for the two enclosures A and B (see Fig. 1) as follows:

$$\begin{aligned} &U = V = \Psi = 0, \quad \Omega = \left(\frac{\partial V}{\partial X}\right)_{X=0}, \quad \theta = 0 \qquad \text{at } X = 0,\\ &U = V = \Psi = 0, \quad \Omega = \left(\frac{\partial V}{\partial X}\right)_{X=1}, \quad \frac{\partial \theta}{\partial X} = 0 \qquad \text{at } X = 1,\\ &U = 1, \quad V = \Psi = 0, \quad \Omega = -\left(\frac{\partial U}{\partial Y}\right)_{Y=0}, \quad \theta = 1 \qquad \text{at } Y = 0. \end{aligned} \tag{12}$$

The boundary conditions for the lower wall of enclosure A (case a) are:

$$U = V = \Psi = 0, \quad \Omega = -\left(\frac{\partial U}{\partial Y}\right)_{Y=-1}, \quad \theta = 0 \qquad \text{at } Y = -1,$$

while that for the upper wall of enclosure B (case b) are:

$$U = V = \Psi = 0, \quad \Omega = -\left(\frac{\partial U}{\partial Y}\right)_{Y=1}, \quad \theta = 0 \qquad \text{at } Y = 1. \tag{13}$$

The vorticity at the non-slip boundary is obtained by a Taylor series out from the wall and is independent of the wall orientation.

The heat transfer rate at steady state is estimated by computing the local Nusselt number on the heated wall:

$$Nu_X = \frac{\dot{Q}_{conv}}{\dot{Q}_{cond}} = -\left(\frac{\partial \theta}{\partial Y}\right)_{Y=0}. \tag{14}$$

The average Nusselt number is obtained by integration of the local Nusselt number over the entire length of the heated wall:

$$N\bar{u} = \frac{\dot{Q}_{conv}}{\dot{Q}_{cond}} = -\int_0^1 \left.\frac{\partial \theta}{\partial Y}\right|_{Y=0} dX. \tag{15}$$

3. Numerical solution

The governing equations (9)–(11) together with the boundary conditions were solved numerically using the method of finite difference, which reduces the continuum problem to a discrete problem prescribed by a system of algebraic equations. The vorticity transport and energy equations were solved using the Alternating Direction Implicit (ADI) method and the stream function equation was solved by the successive over relaxation method. The first and second spatial derivatives of the equations were thereby approximated by the central difference scheme, while the second order upwind difference scheme was used to discretize the convective non-linear terms due to its better stability and convergence of the computation process since the direction of the flow was considered [24]. The resulting systems of linear algebraic equations were solved iterative using successive relaxation method.

At time $t = 0$, the values for the temperature, the stream function, the vorticity, and the velocity components at all the interior grid points were set to zero. The solution algorithm was such that the temperature distribution was foremost determined by solving the energy transport equation. This was followed by the computation of the vorticity and the stream function fields. The wall vorticities were updated from the solution of the stream function equation, while the velocity components were obtained in the dimensionless form from Eq. (6). The steady state was determined by monitoring the convergence of the temperature, stream function, and the vortex fields using the relative error test

$$\frac{\sum_{j=2}^{N}\sum_{i=2}^{M}\left|\Phi_{i,j}^{n+1} - \Phi_{i,j}^{n}\right|}{\sum_{j=2}^{N}\sum_{i=2}^{M}\left|\Phi_{i,j}^{n+1}\right|} \leqslant \delta. \tag{16}$$

The parameter Φ stands for Ψ, θ, or Ω and n denotes the number of iterations. The value of δ used as stated in different literatures varies between 10^{-3} and 10^{-8} [25]. A value of equals 10^{-5} was however used in this work because any further reduction in this value did not yield any change in the results of the computed fields.

4. Results and discussion

Foremost the accuracy and the reliability of the code used in this work were tested by checking the grid refinement sensitivity of the results generated on the average Nusselt number for various Richardson number in a square enclosure. The numerical experiments were performed with uniform grid systems of 41×41, 61×61, 81×81, and 101×101 and the results are presented in Table 1. The results indicate that a grid system of 61×61 is sufficient for the range of Richardson numbers considered in this study in agreement with the findings of Ghasemi and Aminossadati [11]. This was thus used for all simulations in the present work as a compromise between the computation cost, numerical stability, and good field resolution.

Further verification and validation of the present numerical results were done by computing the flow and the temperature fields of on the upper horizontal wall lid-driven square cavity that is thermally insulated on the vertical walls with the upper horizontal wall at higher temperature than the lower one. The values of the minimum and maximum velocity components of the flow field were presented in Table 2 along side with the results of Iwatsu et al. [18], Khanafer and Chamkha [27], and Abdelkhalek [26] for a Grashof number, $Gr = 100$ and Reynolds numbers, $Re = 100$ and 400. A close agreement can be seen between the present results and those of others presented. The computed average Nusselt numbers were also compared in Table 3 with previous results of Abdelkhalek [26], Khanafer et al. [13], Sharif [3], Khanafer and Chamkha [27], and Iwatsu et al. [18] for Grashof number, $Gr = 100$ and various Reynolds numbers. The computed average Nusselt numbers in this work agree very well with the results from these previous works.

The steady state results obtained from the solution of transient equations (9)–(11) subject to the boundary conditions (12) and (13) are now presented in terms of the streamline and isotherm patterns, and the profiles of the velocity, temperature and the local Nusselt number. The results are presented for the two cases considered viz. (a) heating and driving on the upper horizontal wall and (b) heating and driving on the lower horizontal wall. The Reynolds number was fixed at $Re = 100$ for both cases while the values of others problem governing parameters including the aspect ratio,

Table 1
The effect of grid refinement on average Nusselt number for various Richardson number.

Ri	Grid system			
	41×41	61×61	81×81	101×101
0.01	2.00874	2.02400	2.01321	1.97038
0.1	1.25154	1.25543	1.25271	1.24228
1	1.03116	1.03165	1.03129	1.02996
10	1.00319	1.00324	1.00326	1.00308
100	1.00032	1.00033	1.00032	1.00032

Table 2
Comparison of the computed values of the minimum and the maximum horizontal and vertical velocities in the cavity with those of the previous works from Abdelkhalek [26], Khanafer and Chamkha [27], and Iwatsu et al. [18] for Grashof number, $Gr = 100$ at both Reynolds numbers, $Re = 100$ and 400.

	$Re = 100$				$Re = 400$			
	Present results	Abdelkhalek [26]	Khanafer and Chamkha [27]	Iwatsu et al. [18]	Present results	Abdelkhalek [26]	Khanafer and Chamkha [27]	Iwatsu et al. [18]
U_{min}	−0.21198	−0.2147	−0.2122	−0.2037	−0.31871	−0.3104	−0.3099	−0.3197
U_{max}	1.0000	1.0000	1.0000	1.0000	1.00003	1.0000	1.0000	1.0000
V_{min}	−0.251027	−0.2485	−0.2506	−0.2448	−0.441064	−0.4435	−0.4363	−0.4459
V_{max}	0.177125	0.1703	0.1765	0.1699	0.294505	0.2903	0.2866	0.2955

Table 3
Comparison of the average Nusselt number computed in this work with those of the previous works from Abdelkhalek [26], Khanafer et al. [13], Sharif [3], Khanafer and Chamkha [27], and Iwatsu et al. [18] at Grashof number, $Gr = 100$.

Re	Present results	Abdelkhalek [26]	Khanafer et al. [13]	Sharif [3]	Khanafer and Chamkha [27]	Iwatsu et al. [18]
1	1.00033	–	–	–	–	–
100	2.03116	1.9850	2.02	–	2.01	1.94
400	4.02462	3.8785	4.01	4.05	3.91	3.84
500	4.52671	–	–	–	–	–
1000	6.48423	6.3450	6.42	6.55	6.33	6.33

AR, the Richardson number, Ri and the Prandtl number, Pr were varied in the range $1 \leqslant AR \leqslant 4$, $0.1 \leqslant Ri \leqslant 10$, and $10^{-3} \leqslant Pr \leqslant 10$, respectively.

Figs. 2 and 3 illustrate the hydrodynamic and the thermal fields for the two cases for pure convection at the Reynolds number, $Re = 100$, mixed convection for $Ri = 1$ and 10 at fixed Reynolds number, $Re = 100$, and natural convection at $Gr = 10^3$. The flow fields presented in the form of lines of constant stream function, consist of one-cell pattern for forced and natural convections for both cases, while for mixed convection strong two-cell patterns characterized the field for case (a) and a weak second cell evolved at a Richardson number, $Ri = 10$ for case (b). The increase in the convection vigour corresponds to the increase in the value of the stream function. The clustered streamlines near the upper wall for case (a) and lower wall for case (b) both for forced and mixed convection indicate steep velocity gradients in the vertical direction in this region. The temperature fields are strongly influenced by the flow fields as can be seen in Fig. 3. The figures reveal that at the Grashof number, $Gr = 10^3$, the temperature field is characterized by quasi conduction while the isotherms are strongly distorted for forced and mixed convective flow in both cases in the regions where the velocity gradients are steepest. The isotherms are stratified for $Ri = 10$ in case (a).

The influence of the Richardson number on the flow and on the thermal fields is quantified by presenting the plot of the horizontal and vertical velocity components, and temperature profiles across the mid-plane of the cavity as depicted in Figs. 4–6, respectively. The quantitative values of the vertical and the horizontal velocities are the measure of the strength of the flow. The profile of the horizontal velocity presented for Richardson number, $Ri = 0.1$ in Fig. 4(a) compared very well with that of forced convection for Reynolds number, $Re = 100$ in the work of Al-Amiri et al. [23] indicating that the flow is characterized by forced convection at this Richardson number. The figure further shows that the profile for

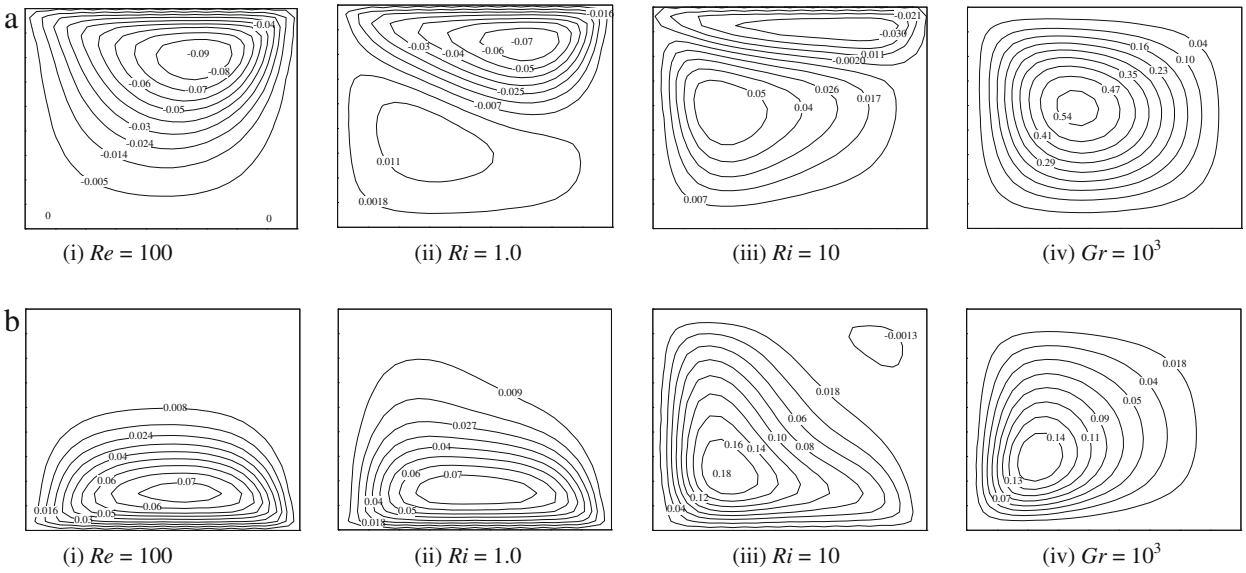

Fig. 2. The flow fields for (i) forced convection, $Re = 100$, (ii) mixed convection, $Ri = 1.0$, (iii) mixed convection, $Ri = 10$, and (iv) natural convection, $Gr = 10^3$ in the square enclosures for cases (a) and (b).

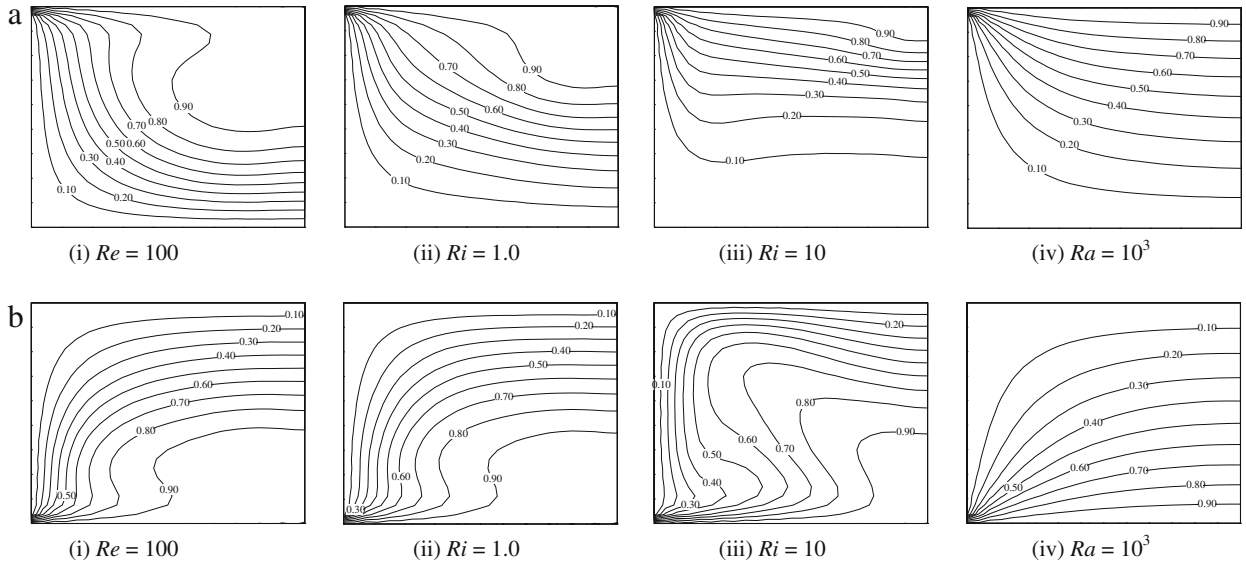

Fig. 3. The temperature fields for (i) forced convection, $Re = 100$, (ii) mixed convection, $Ri = 1.0$, (iii) mixed convection, $Ri = 10$, and (iv) natural convection, $Gr = 10^3$ in the square enclosures for cases (a) and (b).

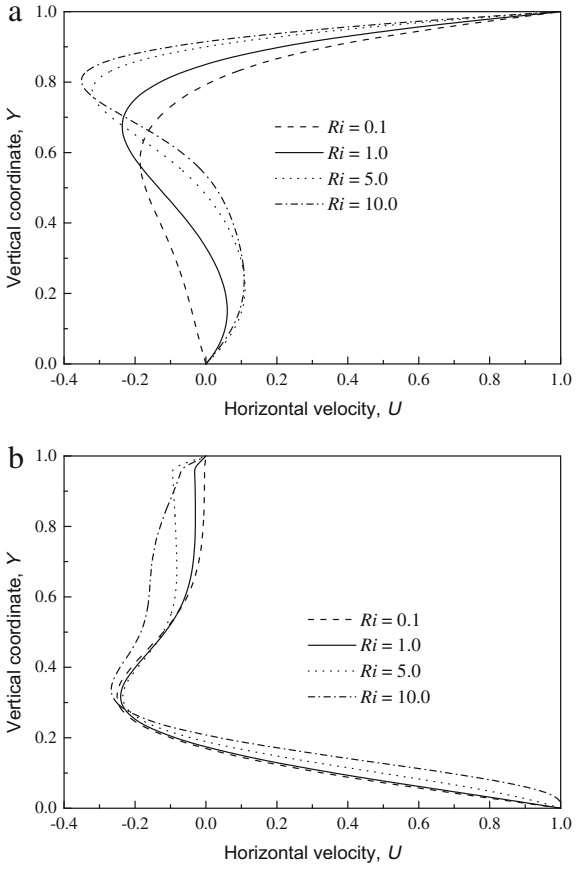

Fig. 4. The effects of the Richardson number, Ri, on the horizontal velocity profiles across the vertical mid-plane, $X = 0.5$, for $Re = 100$ and $AR = 1$ for cases (a) and (b).

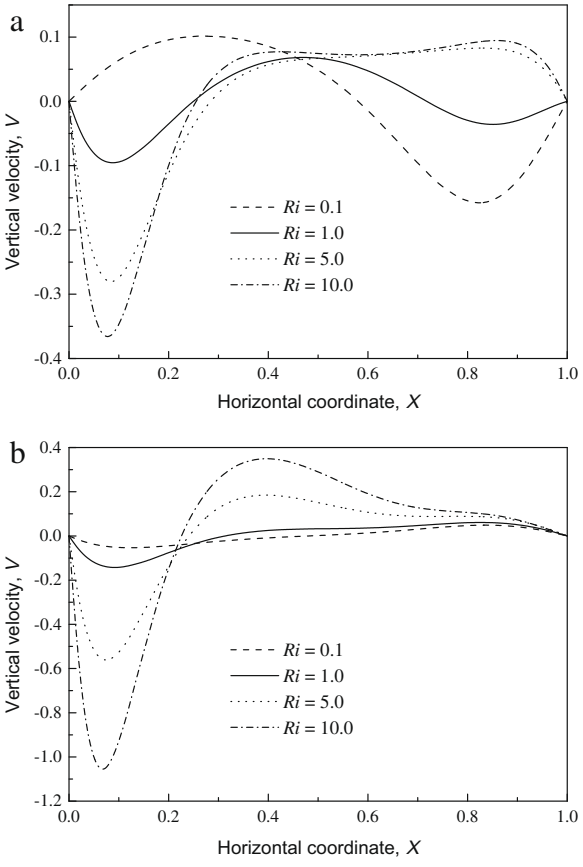

Fig. 5. The vertical velocity profiles across the horizontal mid-plane, $Y = 0.5$, for $Re = 100$ and $AR = 1$ for cases (a) and (b) for various Richardson number, Ri.

$Ri = 0.1$ has one turning point, implying that the flow field consists of unicellular pattern. An increase in the Richardson number leads to dramatic changes in the flow pattern. The profiles for $Ri = 1$, 5, and 10 have two points of inflection indicating that the flow pattern is characterized by two-cell. The vertical velocity profiles illustrated in Fig. 4(b) show a point of inflection. The increase in the Richardson number has small effect on the velocity profiles for this case, which is to be expected since this configuration presents an unstable problem. The vertical velocity profiles presented in Fig. 5 corroborate the flow patterns as a function of Richardson number and the problem configuration as discussed above. Strong

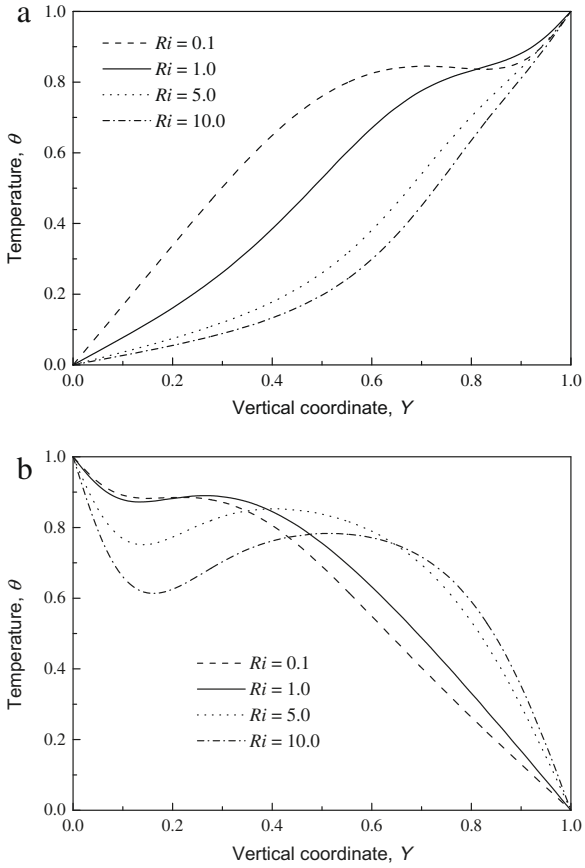

Fig. 6. The effects of the Richardson number on the temperature profiles across the vertical mid-plane, $X = 0.5$, for $Re = 100$ and $AR = 1$ for cases (a) and (b).

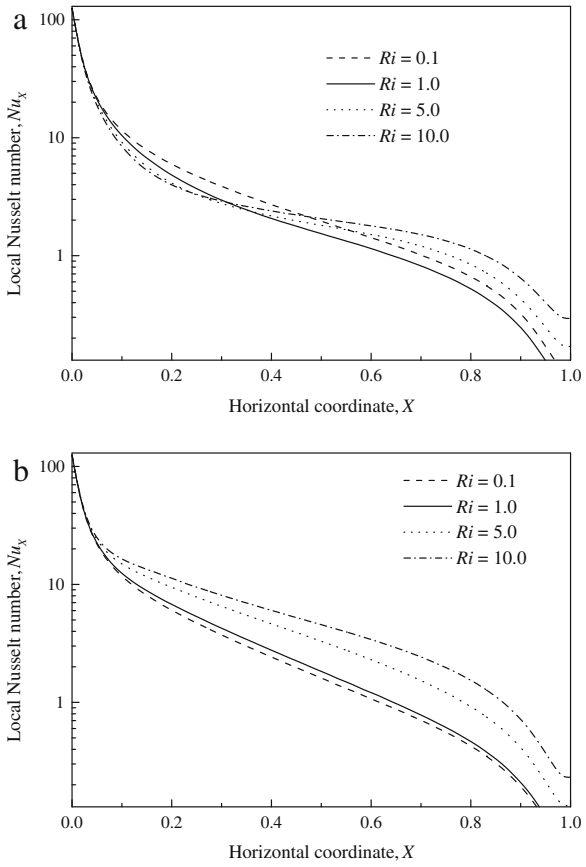

Fig. 7. The effects of the Richardson number, *Ri*, on the local Nusselt number along the horizontal heated wall for $Re = 100$ and $AR = 1$ for cases (a) and (b).

changes in the velocity profiles only occur in the region close to the vertical wall for case (b), while it spans the entire enclosure for case (a).

Fig. 6 illustrates the temperature profiles across the vertical mid-plane of the cavity for the two cases considered for various Richardson numbers. The increase in the Richardson number results in the increase in the effect of the buoyancy force on the convection in the enclosure with the consequent stronger convective heat transfer over the forced convection case. For case (a) the gradient of the temperature curves in the enclosure decreases with the increase in the Richardson number due to the evolution of flow stratification, while converse is the situation for case (b). The implication is that the convective heat transfer within the enclosure in case (a) for a particular Richardson number is weaker than that in case (b).

The profiles of local Nusselt number are presented in Figs. 7–9 to illustrate the influence of the Richardson number, the aspect ratio and the Prandtl number on the heat flux into the enclosure through the heated wall. In all these figures the value of the local Nusselt number predicted at the left end of the heated horizontal wall is high due to the presence of discontinuity in the temperature boundary condition at this edge. The profiles show a monotonic decrease in the local Nusselt number from the high left end value to a small value towards the right end. This trend is consistent with the results of Sharif [3] and Basak et al. [21,28]. Fig. 7 reveals that the effect of the Richardson number on the heat flux profile is stronger for case (b) than for case (a). The profiles for $Ri = 0.1$ and $Ri = 10$ for case (b) form the lower and the upper bound while the curves for other Richardson number within this range run in between them. The stronger flow field close to the moving lid in case (a) compared with that of case (b) causes heat to be conveyed faster away from this wall than in case (b) with the consequence of lower heat flux along the heated wall in case (a) than that at corresponding point in case (b). Fig. 8 compares the influence of the length-to-height aspect ratio of the cavity on the heat flux for a Richardson number, $Ri = 5$. The results show that higher heat flux is predicted for an aspect ratio of unity for the two cases than for other higher aspect ratios. The curves for the aspect ratios of 3 and 4 for case (a) almost fall on each other implying that further increase in the aspect ratio may not bring any reduction in the local heat flux. The heat flux profiles for the aspect ratios higher than unity for case (b) have two points of inflection due to the flow fields that are characterized by two symmetric horizontal cells.

The effects of the Prandtl number on the local Nusselt number profiles for the two cases are similar as illustrated in Fig. 9. For this figure the Reynolds number is fixed at, $Re = 100$ and Grashof number, $Gr = 10^3$ for a square enclosure, while the Prandtl number is varied between 10^{-3} and 10. The curves for $Pr = 10^{-3}$ and $Pr = 10^{-2}$ for the two cases fall on each other implying that the Prandtl number has no effect on the local Nusselt number with the reduction of the number below unity. This result is corroborated by the effect of Prandtl number on the average Nusselt number as reported by Waheed [29]. The overall effect of the increase in the Prandtl number is the increase in the local heat flux which is in agreement with the findings of Basak et al. [21] and Moallemi and Jang [30] on the effect of Prandtl number on the local and the average Nusselt number. This result is plausible since Prandtl number is the ratio of the thermal energy convected to the fluid to the thermal energy conducted within the fluid. If Prandtl number is small, conduction is important and in such a case, the major source of conduction could be at the walls of the enclosure.

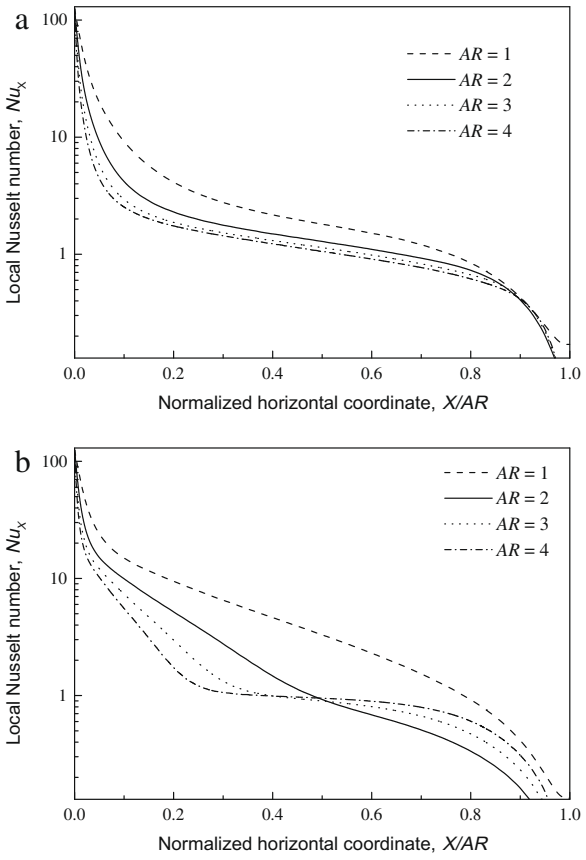

Fig. 8. The effects of the aspect ratio, *AR*, on the local Nusselt number along the horizontal heated wall for $Ri = 5.0$ for cases (a) and (b).

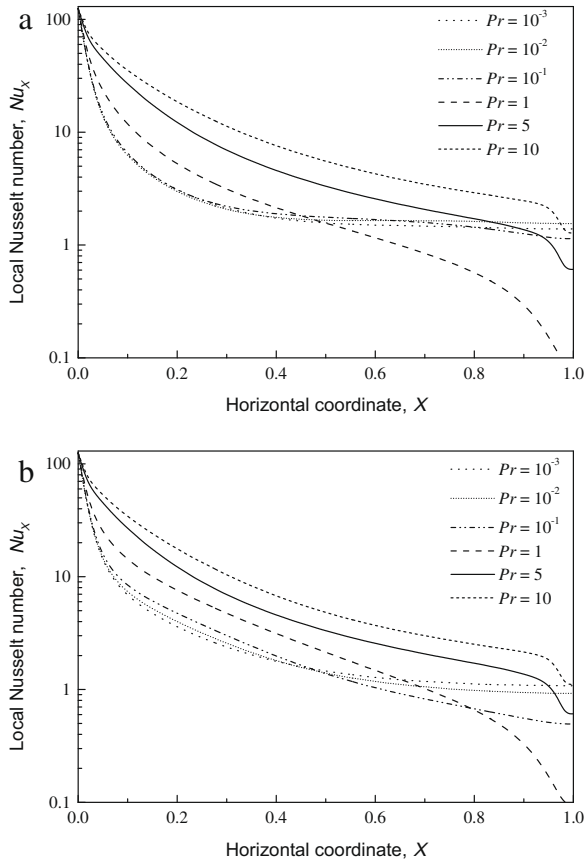

Fig. 9. The effects of the Prandtl number, *Pr*, on the local Nusselt number along the horizontal heated wall for $Gr = 10^3$ and $AR = 1$ for cases (a) and (b).

5. Conclusions

The results of the problem presented in this work were those of the numerical investigations of flow and thermal fields, and heat transfer behaviours by mixed convection in rectangular enclosures driven by horizontal heated wall with the right vertical wall thermally isolated. The other walls of the enclosures are at the ambient temperature. Two flow geometries were investigated: (a) flow driven and heated by the top wall, and (b) flow driven and heated by the bottom wall. The flow governing equations were solved using the central finite difference procedure and the results were validated against published values and found to give very good agreement. The effects of the flow governing parameters on the characteristics of the flow and thermal fields were analysed. The new results show that the flows and the thermal fields have strong dependence on the Richardson number, aspect ratio and the Prandtl number. An increase in the Richardson and Prandtl number, respectively, enhance the fluid flow and energy distribution within the enclosure, and heat flux on the heated wall, while an increase in the aspect ratio suppresses it. The flow pattern and the heat distribution in the enclosure are also function of the flow domain. From the heat flux profiles for case (b), it becomes obvious that a two-cell flow evolves with the increase in the aspect ratio. Several flow characteristics which may prevail in different problems, such as boundary layers, eddies of different sizes and characteristics, and flow instabilities have featured in the problem presented. Consequently more physical insight into various flow problems can be gained from the results of the work which can help to optimise and improve the performance of various industrial processes.

Acknowledgements

The numerical part of this work was carried out during the author's Commonwealth Fellowship at the Department of Mechanical Engineering, University of Bath, Claverton Down, BA2 7AY, United Kingdom, for which he would like to acknowledge both the British Council and the Association of Commonwealth Universities for the financial support, and the University of Bath for the hospitality.

The author would also like to thank anonymous reviewers for critical comments which improved the quality of the manuscript.

References

[1] O. Aydin, Aiding and opposing mechanisms of mixed convection in a shear- and buoyancy-driven cavity, Int. Commun. Heat Mass Transfer 26 (7) (1999) 1019–1028.
[2] Y. Jaluria, Fluid flow phenomena in materials processing – the 2000 Freeman Scholar Lecture, ASME J. Fluids Eng. 123 (2001) 173–210.
[3] M.A.R. Sharif, Laminar mixed convection in shallow inclined driven cavities with hot moving lid on top and cooled from bottom, Appl. Therm. Eng. 27 (2007) 1036–1042.
[4] J.C.-F. Wong, Numerical simulation of two-dimensional laminar mixed-convection in a lid-driven cavity using the mixed finite element consistent splitting scheme, Int. J. Numer. Methods Heat Fluid Flow 17 (1) (2007) 46–93.
[5] P.N. Shankar, M.D. Deshpande, Fluid mechanics in the driven cavity, Annu. Rev. Fluid Mech. 32 (2000) 93–136.
[6] T.M. Jeng, S.C. Tzeng, Heat transfer in a lid-driven enclosure filled with water-saturated aluminum foams, Numer. Heat Transfer A 54 (2008) 178–196.
[7] A. Bahlaoui, A. Raji, R. El Ayachi, Coupled natural convection and radiation in a horizontal rectangular enclosure discretely heated from below, Numer. Heat Transfer A 52 (2007) 1027–1042.
[8] A.A. Mohamad, R. Viskanta, Flow and heat transfer in a lid-driven cavity filled with a stably stratified fluid, Appl. Math. Model. 19 (1995) 465–472.

[9] O. Aydin, W.J. Yang, Mixed convection in cavities with a locally heated lower wall and moving sidewalls, Numer. Heat Transfer A 37 (2000) 695–710.
[10] H.F. Oztop, I. Dagtekin, Mixed convection in two-sided lid-driven differentially heated square cavity, Int. J. Heat Mass Transfer 47 (2004) 1761–1769.
[11] B. Ghasemi, S.M. Aminossadati, Comparison of mixed convection in a square cavity with an oscillating versus a constant velocity wall, Numer. Heat Transfer A 54 (2008) 726–743.
[12] W.-J. Luo, R.-J. Yang, Multiple fluid flow and heat transfer solutions in a two-sided lid-driven cavity, Int. J. Heat Mass Transfer 50 (2007) 2394–2405.
[13] K.M. Khanafer, A.M. Al-Amiri, I. Pop, Numerical simulation of unsteady mixed convection in a driven cavity, using an externally excited sliding lid, Eur. J. Mech. B Fluids 26 (2007) 669–687.
[14] A.K. Prasad, J.R. Koseff, Combined forced and natural convection heat transfer in a deep lid-driven cavity flow, Int. J. Heat Fluid Flow 17 (1996) 460–467.
[15] J.R. Koseff, R.L. Street, The lid-driven cavity flow: a synthesis of qualitative and quantitative observations, J. Fluids Eng. 106 (1984) 390–398.
[16] S.J. Tsorng, H. Capart, D.C. Lo, J.S. Lai, D.L. Young, Behaviour of macroscopic rigid spheres in lid-driven cavity flow, Int. J. Multiphase Flow 34 (2008) 76–101.
[17] P.M. Ligrani, S. Choi, Mixed convection in straight and curved channels with buoyancy orthogonal to the forced flow, Int. J. Heat Mass Transfer 39 (12) (1996) 2473–2484.
[18] R. Iwatsu, J.M. Hyun, K. Kuwahara, Mixed convection in a driven cavity with a stable vertical temperature gradient, Int. J. Heat Mass Transfer 36 (6) (1993) 1601–1608.
[19] H.F. Oztop, C. Sun, B. Yu, Conjugate-mixed convection heat transfer in a lid-driven enclosure with thick bottom wall, Int. Commun. Heat Mass Transfer 35 (2008) 779–785.
[20] A. Al-Amiri, K. Khanafer, J. Bull, I. Pop, Effect of sinusoidal wavy bottom surface on mixed convection heat transfer in a lid-driven cavity, Int. J. Heat Mass Transfer 50 (2007) 1771–1780.
[21] T. Basak, S. Roy, P.K. Sharma, I. Pop, Analysis of mixed convection flows within a square cavity with uniform and non-uniform heating of bottom wall, Int. J. Therm. Sci. 48 (2009) 891–912.
[22] H. Schlichting, K. Gersten, Boundary Layer Theory, eighth ed., Springer Verlag, Berlin, 2003 (Chapter 3).
[23] A.M. Al-Amiri, K.M. Khanafer, I. Pop, Numerical simulation of combined thermal and mass transport in a square lid-driven cavity, Int. J. Therm. Sci. 46 (2007) 662–671.
[24] K. Küblbeck, G.P. Merker, J. Straub, Advanced numerical computation of two-dimensional time-dependent free convection in cavities, Int. J. Heat Mass Transfer 23 (1980) 203–217.
[25] P.J. Roache, Computational Fluid Dynamics, Hermosa Publishers, Albuquerque, NM, 1976. p. 174.
[26] M.M. Abdelkhalek, Mixed convection in a square cavity by a perturbation technique, Comput. Mater. Sci. 42 (2008) 212–219.
[27] K.M. Khanafer, A.J. Chamkha, Mixed convection flow in a lid-driven enclosure filled with a fluid-saturated porous medium, Int. J. Heat Mass Transfer 42 (1999) 2465–2481.
[28] T. Basak, S. Roy, S.K. Babu, I. Pop, Finite element simulations of natural convection flow in an isosceles triangular enclosure filled with a porous medium: effects of various thermal boundary conditions, Int. J. Heat Mass Transfer 51 (2008) 2733–2741.
[29] M.A. Waheed, An approach to the simulation of natural convective heat transfer between two horizontal cylindrical annuli, Numer. Heat Transfer A 53 (2) (2008) 323–340.
[30] M.K. Moallemi, K.S. Jang, Prandtl number effects on laminar mixed convection heat transfer in a lid-driven cavity, Int. J. Heat Mass Transfer 35 (1992) 1881–1892.